remote sensing

MDPI

Article

Using Remote and Proximal Sensing Data and Vine Vigor Parameters for Non-Destructive and Rapid Prediction of Grape Quality

Hongyi Lyu [1], Miles Grafton [1,*], Thiagarajah Ramilan [1], Matthew Irwin [1], Hsiang-En Wei [1] and Eduardo Sandoval [2]

[1] School of Agriculture and Environment, Massey University, Palmerston North 4410, New Zealand; h.lyu@massey.ac.nz (H.L.); t.ramilan@massey.ac.nz (T.R.); m.e.irwin@massey.ac.nz (M.I.); h.wei1@massey.ac.nz (H.-E.W.)

[2] Massey Agri-Food (MAF) Digital Laboratory, Massey University, Palmerston North 4410, New Zealand; e.a.sandoval@massey.ac.nz

* Correspondence: m.grafton@massey.ac.nz

Abstract: The traditional method for determining wine grape total soluble solid (TSS) is destructive laboratory analysis, which is time consuming and expensive. In this study, we explore the potential of using different predictor variables from various advanced techniques to predict the grape TSS in a non-destructive and rapid way. Calculating Pearson's correlation coefficient between the vegetation indices (VIs) obtained from UAV multispectral imagery and grape TSS resulted in a strong correlation between OSAVI and grape TSS with a coefficient of 0.64. Additionally, seven machine learning models including ridge regression and lasso regression, k-Nearest neighbor (KNN), support vector regression (SVR), random forest regression (RFR), extreme gradient boosting (XGBoost), and artificial neural network (ANN) are used to build the prediction models. The predictor variables include the unmanned aerial vehicles (UAV) derived VIs, and other ancillary variables including normalized difference vegetation index (NDVI_proximal) and soil electrical conductivity (EC_a) measured by proximal sensors, elevation, slope, trunk circumference, and day of the year for each sampling date. When using 23 VIs and other ancillary variables as input variables, the results show that ensemble learning models (RFR, and XGBoost) outperform other regression models when predicting grape TSS, with the average of root mean square error (RMSE) of 1.19 and 1.2 °Brix, and coefficient of determination (R^2) of 0.52 and 0.52, respectively, during the 20 times testing process. In addition, this study examines the prediction performance of using optimized soil adjusted vegetation index (OSAVI) or normalized green-blue difference index (NGBDI) as the main input for different machine learning models with other ancillary variables. When using OSAVI-based models, the best prediction model is RFR with an average R^2 of 0.51 and RMSE of 1.19 °Brix, respectively. For NGBDI-based model, the RFR model showed the best average result of predicting TSS were a R^2 of 0.54 and a RMSE of 1.16 °Brix, respectively. The approach proposed in this study provides an opportunity to grape growers to estimate the whole vineyard grape TSS in a non-destructive way.

Keywords: wine grape; vegetation indices; UAV multispectral imagery; sugar content

Citation: Lyu, H.; Grafton, M.; Ramilan, T.; Irwin, M.; Wei, H.-E.; Sandoval, E. Using Remote and Proximal Sensing Data and Vine Vigor Parameters for Non-Destructive and Rapid Prediction of Grape Quality. *Remote Sens.* **2023**, *15*, 5412. https://doi.org/10.3390/rs15225412

Academic Editors: Ce Zhang and Desheng Liu

Received: 11 September 2023
Revised: 31 October 2023
Accepted: 17 November 2023
Published: 19 November 2023

1. Introduction

Viticulture is an important sector within the New Zealand horticultural system, with a total vineyard production area extending over 41,000 ha [1]. In New Zealand, conventional vineyards typically employ uniform management practices. However, studies have demonstrated the spatial and temporal variation in vine vigor, grape yield, and quality within the vineyard scale [2,3]. With uniform management, a single application rate of fertilizers, pesticides and irrigation are used for the entire vineyard. As a consequence of uniform management, parts of the field are likely to receive too little and others too much input.

This could have negative impacts on the environment, such as groundwater pollution, soil degradation and increase pressure from weeds and pests [4]. Precision viticulture (PV) provides an opportunity for grape growers to understand and manage the vineyard spatial variability by using remote sensing data and geostatistical analysis. Remote sensing allows viticulturists to continuously monitor spatial and temporal variation in soil properties and vine growth status [5]. This is particularly relevant for New Zealand wine growers who need to understand and manage vineyard variability to increase grape quality and achieve sustainable viticulture.

Remote sensing is the process of acquiring spectral data remotely from several platforms including ground vehicles, aircraft, uncrewed aerial vehicles (UAV), and satellites. In recent years, remote sensing has been widely applied in PV to evaluate the vineyard spatial variability of vine vigor, nutrient status, wine water status, and grape yield and quality [5–7]. Satellite platforms with multispectral cameras, such as Sentinel-2 with 10 m pixel resolution and Landsat 8 with 30 m pixel resolution, have been used on a regional scale to predict grape yield [8,9]. However, low spatial resolution satellite imagery makes it difficult to monitor vine growth status on a vineyard block scale without bias, as a single pixel of satellite imagery often mixes inter-row crops and bare soil. UAV and aircraft sensors carrying multispectral or hyperspectral cameras have provided high spatial resolution imagery on a vineyard scale. For example, Carrillo et al. found a linear relationship between berry weight and NDVI derived from multispectral airborne imagery [10]. In addition, Lamb et al. found a strong correlation between berry quality parameters and multispectral airborne imagery obtained at veraison [7]. However, the operational cost of aircraft is very expensive. Compared to other platforms, UAV provide an interesting alternative approach for PV, as it can provide high spatial resolution images at a lower cost [11]. For example, García-Fernández et al. found a significant correlation between RGB-based vegetation indices derived from UAV imagery and berry quality [12]. Wei et al. found the VIs-derived UAV multispectral imagery combined with other environmental variables can predict grapevine water status (stem water potential Ψstem), with the RMSE of 138 kPa [13]. In addition to remote sensing, proximal sensors have demonstrated their capability to explore the spatial and temporal variation of vine growth status within the vineyard scale. Bramley et al. used a handheld proximal sensor (Crop Circle™, Holland Scientific, Lincoln, Nebraska, USA) and an EM38 electromagnetic soil sensor (Geonics Ltd, Mississauga, Ontario, Canada) to explore the spatial variability of vine vigor and yield as well as soil texture on a vineyard block scale, while neither ECa nor VIs derived from proximal sensor were good predictors of grape yield [3]. Their result also indicated that EC_a and VIs significantly correlated with vine vigor. Furthermore, a portable hyperspectral spectroradiometer can be used to predicted the vine growth status and grape quality within the vineyard scale [14,15].

One of the main objectives of PV is selective harvesting. A major reason for wishing to do this, considering the variability of vineyards, is to harvest berries with consistent quality during the harvest stage resulting in higher profit margins from wine [16]. In New Zealand, sugar content commonly describes the quality of wine grapes at harvest. The sugar content relates to the alcohol level of wine during the fermentation process. The traditional method used in monitoring wine grape sugar content is to perform sample-based laboratory destructive analysis which can be time consuming and an expensive process. In recent years, remote and proximal sensors have been used to monitor grape sugar content [12,17,18]. For example, Benelli et al. used a push broom hyperspectral camera mounted on a vehicle to predict the sugar content of wine grapes [17]. In addition, Kasimati et al. used NDVI obtained from proximal and remote sensing during different growing stages to predict grape sugar content with R^2 values of 0.61. Presently, the increase in computing power and advanced sensing techniques enable more accurate prediction of grape quality, helping grape growers assess grape quality before harvest and thus develop a selective harvesting plan.

Previous research has been conducted using Pearson's correlation coefficient and machine learning techniques to explore the relationship between spectral index data and vine growth status, yield, and berry quality parameters. Pearson's correlation coefficients have been constructed to select key spectra indices relevant to the grape sugar content [12]. Machine learning techniques have been constructed to model both linear and non-linear relationships between spectral index data and vine growth status, yield, and berry quality. One study used an artificial neural network (ANN) to predict the table grape yield through different vegetation indices (VIs) obtained from satellite remote sensing [9]. In regard to studies conducted in predicting berry quality parameters, many studies used hyperspectral imaging systems to predict various quality parameters such as sugar content, pH, and titratable acidity through different machine learning techniques [19]. However, most of these studies used remote or proximal sensing to directly measure berries or clusters. Few studies have predicted grape quality through the VIs derived from canopy or leaf level. For example, Kasimati et al. achieved good prediction accuracy with R^2 values of 0.65 for grape sugar content using NDVI and automated machine learning [20]. The VIs measured from vine canopy or leaves can reflect the vine vigor, water status, and nutrient status [5,14,21]. Thus, it is important to explore the possibility of using the combination of VIs and machine learning techniques to predict grape quality parameters.

The aims of this study are to (1) create an alternative method to predict grape sugar content thorough VIs, derived from proximal and remote sensing, and other ancillary environmental variables during different growth stages, and (2) to determine the ability of different machine learning techniques in predicting grape sugar content.

2. Methods

2.1. Study Sites

The study research sites were conducted in two commercial wine grape vineyard blocks on the Palliser Estate located in Martinborough, New Zealand (175.45235°E 41.21119°S, WGS 84). The study vineyards are named Hua Nui (HN) and Pencarrow (PN). The variety used in the study areas was Pinot Noir which were planted in 1998–2000 for winemaking. The research sites selected for data collection were 3.31 ha for HN and 7.51 ha for PN. The wine grapes in study sites were trained with two-cane vertical shoot positioning. Inter- and intra-row planting space is 2.2 and 1.7 m for HN, and 2.2 and 1.8 m for PN. The region of Martinborough has a mild coastal climate with an average temperature of 18 °C. The soil in the vineyards are mostly clay and silty loams, which are known to have moderate soil water holding capacity. Vine phenology in research vineyards is shown in Table 1. The vineyard manager is responsible for managing the vines and applied all inputs.

Table 1. Vine phenology in the study vineyards.

Vine Phenology	Date
Budburst	September, October
Leaf development	October, November
Inflorescence emergence	November
Flowering	November, Early December
Fruit set and fruiting	December, January
Veraison	Late January, February
Harvest	March, April

2.2. Grape Sugar Content Data Acquisition

Wine grapes were manually harvested between 20 February and 14 March 2023 (from veraison to harvest time). Three berries from a single bunch were randomly selected from each sampling vine. Table 2 shows the number of sampling vines from each measurement date. During each measurement, the location of the sampling vine's trunk was recorded by a global navigation satellite system (GNSS) with real-time kinematic (RTK) correction

(model: GPS1200+, Leica Geosystems AG., Heerbrugg, Switzerland). Figure 1 shows the sampling locations in each vineyard. After acquiring grape berries, total soluble solids (TSS) expressed in °Brix, was chosen as a proxy for grape sugar content and measured by using a portable digital refractometer (PAL-ALPHA Digital Refractometer, ATAGO CO., LTD, Tokyo, Japan). The sugar content of each sampling vine was determined by calculating the mean of the three measurements taken per sampled vine. The weather during collecting samples period is shown in Figure 2.

Table 2. The number of sampling vines in each measurement day.

Vineyard	20 February	26 February	2 March	6 March	14 March
Pencarrow	6	25	37	32	18
Hua Nui	25	36	14	30	13

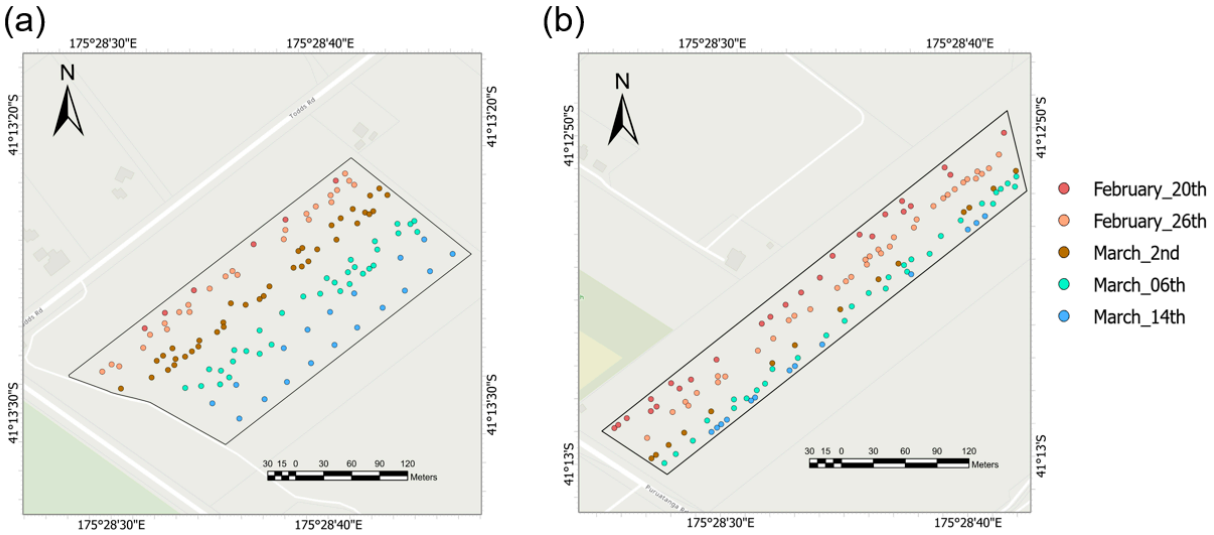

Figure 1. The location of sampling vines in PN (**a**); HN (**b**). (Points represent the location of sampling vines).

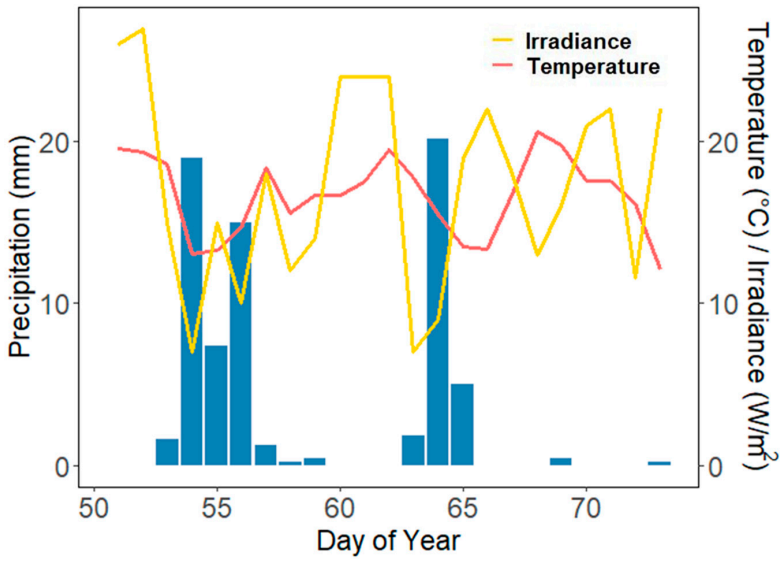

Figure 2. Total daily precipitation, average temperature, and irradiance recorded by on-site weather station (blue bar represents the precipitation).

2.3. Canopy and Leaf Reflectance Data Acquisition

Multispectral imagery was acquired by DJI P4 Multispectral (Da-Jiang Innovations, Shenzhen, China) between 11.00 and 14.00 under stable weather conditions and a clear sky on the 14 December 2022. The DJI P4 Multispectral was gimbal equipped, with a 6-camera array, one camera is an RGB camera, designed for visible light and capturing standard photos, while the remaining five cameras are dedicated to capturing 2 MP images, at various wavelengths: near-infrared, red-edge, red, green, and blue, with centre wavelengths at 840 nm, 730 nm, 650 nm, 560 nm, and 450 nm, and bandwidth of ±26 nm, ±16 nm, ±16 nm, ±16 nm, and ±16 nm, respectively. The DJI P4 flew at 80 m height capturing images with a spatial resolution of 4.2 cm for PN, and some at 84.9 m resulting in 4.5 cm spatial resolution imagery for HN. The DJI P4 is equipped with an integrated sunlight sensor that records irradiance during flight. This sensor captures data in the same bands as the multispectral sensor, which is used for radiometric calibration purposes. In addition, radiometric calibration was performed on the image blocks, using reference images acquired from a calibrated reflectance panel (Seattle, WA, USA). To assure the accuracy of the image, several ground control points were recorded by GNSS-RTK correction in each vineyard during flight for geometric correction. Photogrammetric processing was applied to the georeferenced multispectral images using Pix4Dmapper (Pix4D SA, Lausanne, Switzerland). The digital surface models (DSM), digital terrain models (DTM), and reflectance maps of the study sites were created by Pix4Dmapper.

Due to discontinuous vegetation surfaces for the vineyard features, it becomes essential to differentiate between the pixels belonging to the vine canopy and those in the inter-row spacing. The process of detecting vine rows consists of the following steps: (1) NDVI were calculated by band math function in ENVI 5.6 (Research Systems Inc., Boulder, CO, USA), producing a greyscale image for each study site; (2) then, a global threshold was implemented on the NDVI images to generate a binary image based on Otsu's method (Otsu threshold value is 0.535); (3) a single greyscale image was calculated from subtraction of the DTM to the DSM for each study site; (4) then, a height threshold of 0.9 m was implemented on the greyscale images to generate a binary image [13]. The height threshold was dependent on the vineyards' architecture; (5) then these two binary images were converted to a feature map by ArcGIS Pro 2.9 (ESRI, Redlands, CA, USA); (6) then, using the "Clip" tool in ArcGIS pro to extract the overlapping portion of these two features; (7) using the vine row feature map as a mask layer to retain the original multispectral images (Figure 3).

We located the image pixels that corresponded to the 236 sampling points by selecting pixels on both sides of each sampling point, considering the vine spacing within each vineyard. From these pixels, we extracted reflectance values, averaged them, and subsequently calculated the VIs using the formulas outlined in Table 3.

Leaf reflectance data was measured during 17 February 2023 to record the NDVI of the grapevines' leaves. Three leaves in each sampling vine were randomly selected and scanned using a handheld RapidSCAN CS-45 (Holland Scientific Inc., Lincoln, NE, USA) to record these three leaves NDVI value (NDVI_proximal). The average of the three leaves NDVI values (NDVI_proximal) was used to represent the sampling vine growth status during veraison.

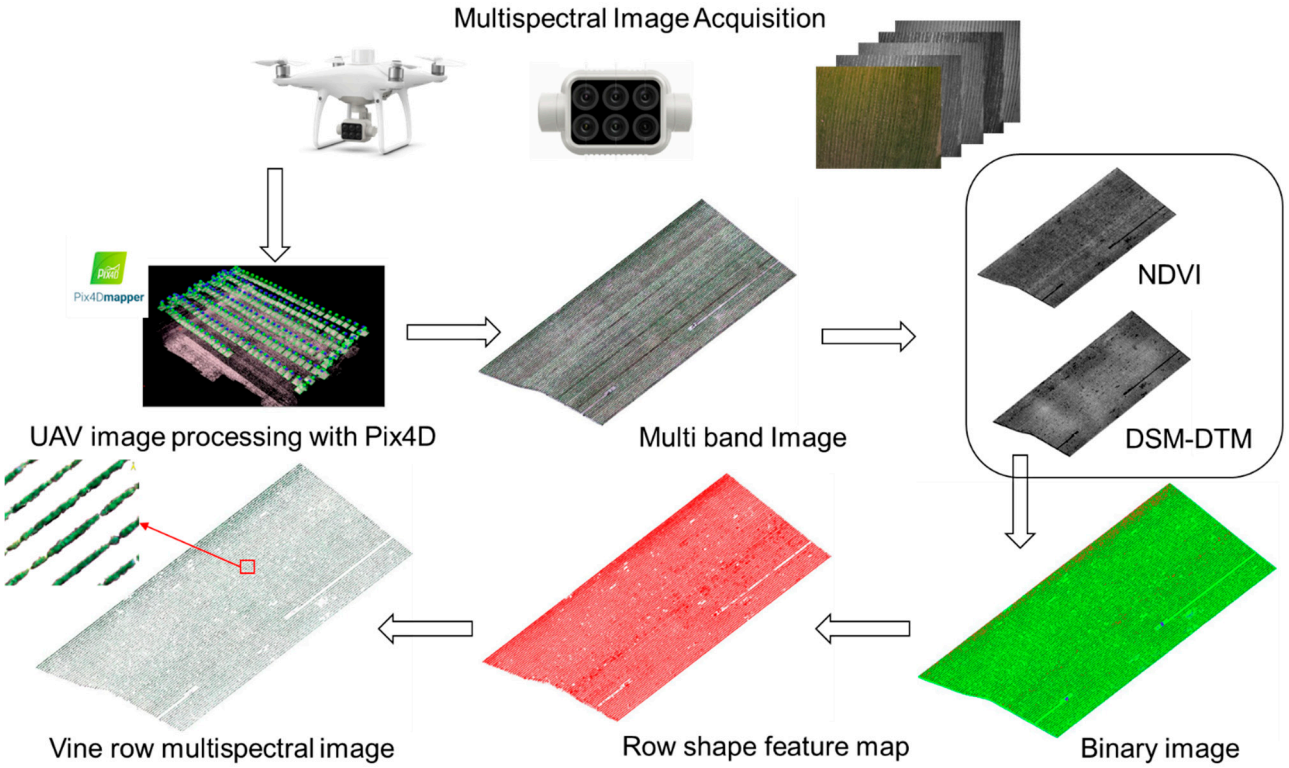

Figure 3. Vine row segmentation workflow.

Table 3. The spectral indices used in this study.

Vegetation Indices	Formula	Reference
PCD	NIR/Red	[22]
NDVI	$(NIR - Red)/(NIR + Red)$	[23]
GNDVI	$(NIR - Green)/(NIR + Green)$	[24]
MSR	$\left(\left(\frac{NIR}{Red}\right) - 1\right)/\sqrt{\left(\left(\frac{NIR}{Red}\right) + 1\right)}$	[25]
MSAVI	$\frac{2 \times NIR + 1 - \sqrt{(2 \times NIR + 1)^2 - 8 \times (NIR - Red)}}{2}$	[25]
RDVI	$(NIR - Red)/\sqrt{(NIR + Red)}$	[25]
OSAVI	$(1 + 0.16)\frac{NIR - Red}{NIR + Red + 0.16}$	[25]
R/B index	$Red/Blue$	[26]
R/G index	$Red/Green$	[26]
NGRDI	$(Green - Red)/(Green + Red)$	[26]
NPCI	$(Blue - Red)/(Blue + Red)$	[26]
VARI	$(Green - Red)/(Green + Red - Blue)$	[27]
Clgreen	$NIR/Green - 1$	[26]
ARI	$Green^{-1} - Rededge^{-1}$	[28]
MARI	$\left(Green^{-1} - Rededge^{-1}\right) \times NIR$	[28]
CLREDEDGE	$(NIR/Rededge) - 1$	[29]
MCARI	$((Rededge - Red) - 0.2 \times (Rededge - Green)) \times (Rededge/Red)$	[29]
NDRE	$(NIR - Rededge)/(NIR + Rededge)$	[29]
EVI	$2.5 \times (NIR - Red)/(NIR + 6 \times Red - 7.5 \times Blue + 1)$	[30]
NGBDI	$(Green - Blue)/(Green + Blue)$	[31]
G%	$Green/(Red + Green + Blue)$	[31]
REGI	$(Rededge - Green)/(Rededge + Green)$	[32]
RERI	$(Rededge - Red)/(Rededge + Red)$	[32]

2.4. Vine Vigour Parameter Acquisition

The trunk circumference (TC) was chosen as a proxy for vine vigor. The trunk circumference of all of the vines was measured 10 cm above the graft union and 10 cm below the head of the vine with the paper ruler during the bud and leaf growing stage. These two measurements per sampled vine were averaged to represent the vine vigor [33].

2.5. Soil and Terrain Data Acquisition

Many studies indicated that soil electrical conductivity (EC_a) can be used to assess soil texture types and water content [34,35]. Soil EC_a is widely used to explore the spatial variation in soil properties within the vineyards [33]. In addition, one study showed that soil EC_a is directly related to vine water status, berry weight, and sugar content [36]. In this study, an electromagnetic induction sensor EM38-MK2 (Geonics Ltd., Mississauga, ON, Canada) was used to assess the soil EC_a in the study area during 27 May 2021. The EM38-MK2 was operated in the vertical dipole mode, capturing integrated EC_a measurements at a depth of approximately 1.5 m. The EM38-MK2 was towed at the back of an all-terrain vehicle, maintaining a distance of less than 0.2 m between the instrument and the vehicle. To ensure accurate georeferencing of all point data from the EC_a (mS/m) survey, a Trimble Yuma tablet equipped with an onboard GPS receiver (model: Yuma, Trimble) accurate to 2–4 m, was utilized. Soil EC_a points were measured at intervals of approximately 3–10 m along transects, with a 10 m spacing between individual measurements.

The elevation (m) and slope (degree) data for the study site were obtained from the 'Wellington LiDAR 1 m DEM (2013–2014)' layer. This dataset was made accessible through the Land Information New Zealand data service (https://data.linz.govt.nz/, accessed on 28 July 2023). This digital elevation model (DEM) has a resolution of 1 m and was created using aerial LiDAR data captured between 2013 and 2014, encompassing the study vineyards.

2.6. Geostatistical Analysis

The application of geostatistics in PV has been undertaken in many studies [3,33]. The purpose of geostatistics is describing spatial autocorrelation of a regionalized variable (the georeferenced data) and uses this information to predict the values of the variable across an entire field by Kriging. The central tool in geostatistics is the variogram, which is a set of semi-variances plotted against the lag distances between the measurements to describe the way in which a property varies from place to place. Experimental variograms were computed using R statistical software (R Core Team, version 4.2.2) with the package "gstat" by the Matheron's method of moments, as in the following formula:

$$\gamma(h) = \frac{1}{2m(h)} \sum_{i=1}^{m(h)} \left[Z_x - Z_{(x+h)} \right]^2$$

where $2m(h)$ is the number of paired comparisons at the lag interval h, Z_x, and $Z_{(x+h)}$ are the values of the property at two locations separated by distance h.

After computing the experimental variogram, the experimental variogram based on a suitable mathematical model. The best fitting mathematical model was selected based on the lowest residual sum of squares (RSS). The parameters of the fitted variogram were used to interpolate the soil EC_a, slope, and elevation value based on ordinary Kriging by using ArcGIS Pro 2.9 (ESRI, Redlands, CA, USA). The soil EC_a values less than 0 mS/m were removed before doing geostatistical analysis. The Kriging interpolation images were then exported to a raster layer with the same gride size as used by the multispectral UAV image. For each sampling vine, the mean values of soil EC_a, elevation, and slope were computed using "zonal statistics as table" in ArcGIS Pro 2.9.

2.7. Machine Learning Model

Different machine learning models were performed to predict the sugar content. The input variables include, canopy reflectance data, leaf reflectance data, TC, soil EC_a, elevation, slope, and day of year for sampling date (DOY). The machine learning models used; included regularized regression, k-Nearest Neighbors (KNN), support vector regression (SVR), random forest regression (RFR), XGBoost, and ANN.

Regularized regression: regularized regression is used to explore the linear relationship between input and output variable, when the data set contain more features than observations. In addition, it is suitable for the analysis of multicollinearity among the features. The objective function of a regularized regression is in the following formula:

$$minimize\left(\sum_{i=1}^{n}(y_i-\hat{y}_i)^2+P\right)$$

where n is the sample number, y_i is the measured truth value of the ith sample, $\hat{y}_i$ is the predicted value of the ith sample, P is the penalty term.

In this study, we used ridge penalty and lasso penalty to build the linear relationship between input and output variables. When using the ridge penalty, the formula of penalty parameters is

$$P=\lambda\sum_{j=1}^{p}\beta_j^2$$

When using the lasso penalty, the formula of penalty parameters is

$$P=\lambda\sum_{j=1}^{p}|\beta_j|$$

where $\lambda \geq 0$ is a tuning parameter, p is the feature number, β_j is the regression coefficient of the jth feature.

KNN: It aims to identify the k most similar instances from a training dataset to predict the target value of a new data point. The Euclidean distance metric are commonly used to determine the similarity between observations. The formula of Euclidean distance is

$$\sqrt{\sum_{j=1}^{p}\left(x_{aj}-x_{bj}\right)^2}$$

where x_a and x_b represent the observations, j represents the feature, p represents the feature number.

SVR: Support vector machine (SVM) try to find a hyperplane in an N-dimensional space (N-the number of features) that "best" classify the two classes. Hyperplane represents a decision boundary that help classify the data points. SVR is an extended tool of SVM to solve regression problems.

RFR: It is an ensemble learning model which combines the multiple decision trees on different subsets of the training data (bootstrap samples), and then averaging their predictions to achieve more accurate and robust regression results.

XGBoost: It combines gradient boosting with regularization techniques, creating a boosted ensemble of decision trees. XGBoost optimizes model predictions by fitting negative gradients of the loss function during each boosting iteration.

ANN: It consists of interconnected nodes called neurons organized into layers: an input layer, one or more hidden layers, and an output layer. Each neuron receives input data, performs computations, and passes the results to the next layer through weighted connections. Activation functions introduce non-linearity and enable ANN to learn complex relationships in data. In this study, we use a single layer neural network to predict the TSS based on input variables.

To evaluate the model's prediction performance, the dataset is divided into training and test sets with the ratio of 7:3. This process was repeated 20 times with different data splits to improve the estimated performance of study models. The performance of machine learning models is affected by their hyperparameters. Thus, it was important to tune the hyperparameters. Bayesian hyperparameter optimization was used on the training set with 10-fold cross-validation to search for the best combination of hyperparameters based on the root mean square error (RMSE). In addition, the coefficient of determination (R^2) and RMSE were selected to compare the performance of different machine learning models on the test set. The Waller–Duncan test was used to conduct multiple comparisons between different machine learning models. The formula of R^2 and RMSE was as follows:

$$R^2 = 1 - \frac{\sum_{i=1}^{n}(y_i - \hat{y}_i)^2}{\sum_{i=1}^{n}(y_i - \overline{y})^2}$$

$$RMSE = \sqrt{\frac{1}{n}\sum_{i=1}^{n}(y_i - \hat{y}_i)^2}$$

where n is the number of sampling vines, y_i is the measured TSS value of the ith vine sample, $\overline{y}$ is the mean measured TSS value, $\hat{y}_i$ is the model predicted TSS value of the ith vine sample.

3. Results

3.1. Variation in Total Soluble Solids

Both vineyards were measured five times from veraison in late February to harvest in middle March. Measuring TSS in this period is crucial for assessing grape maturity and, consequently, making informed decisions about selecting the optimal harvest day. Figure 4 showed the variation in TSS collected from 236 vines across two distinct vineyards, along with the distribution of these measurements for each sampling date. The grape TSS values ranged from 12.8 to 21.2 °Brix during the study period. The extensive range of data within the dataset facilitated the construction of a robust calibration model. The grape TSS values increased rapidly from 2–14 March suggesting a gradual progression towards ripeness as TSS accumulate. It is worth noting that the TSS measured on 20 and 26 February were higher compared to those of 2 March. One possible explanation is the variability of sample collection locations lead to spatial variation in grape TSS. In addition, the height of the boxplot and the magnitude of the interquartile range represent the spatial variability of TSS within each vineyard during different measurement dates (Figure 4).

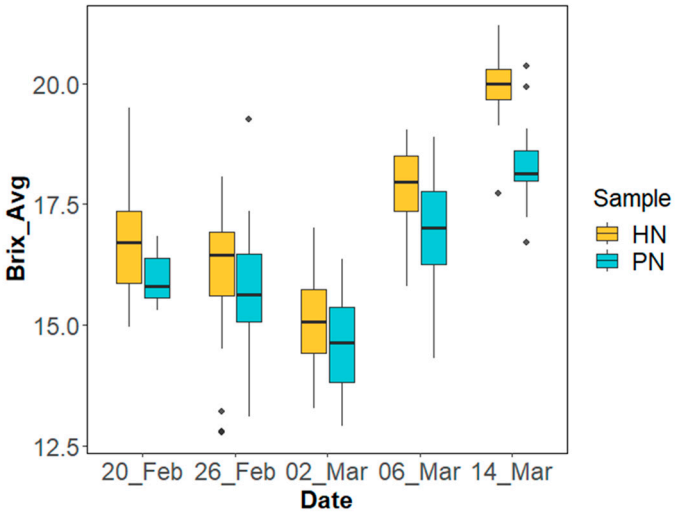

Figure 4. The boxplot of grape TSS during study period (diamond records outliers).

3.2. Pearson's Correlation Coefficient between VIs and TSS

In this study, 23 VIs frequently used in viticulture were calculated based on the red, red edge, green, blue, and near infrared (NIR) bands of the UAV multispectral images. The Pearson's correlation coefficient was used to explore the relationship between VIs and grape TSS, to check the potential of using UAV multispectral images to predict the grape quality. In order to mitigate the influence of different sampling dates on grape TSS content, we calculated the Pearson's correlation coefficient between VIs and grape TSS for each respective sampling date (Figure 5). When the grapes reached the harvest stage, most of VIs showed a strong correlation with grape TSS with the absolute value of the Pearson's correlation coefficient, greater than 0.5. Among all the VIs, optimized soil adjusted vegetation index (OSAVI) had the maximum correlation with grape TSS, with a coefficient of 0.64 during the harvest stage. This was followed by renormalized difference vegetation index (RDVI), enhanced vegetation index (EVI), and anthrocyanin reflectance index (ARI) with the absolute value of the Pearson's coefficient greater than 0.62 during the harvest stage. The NDVI and PCD which are widely used in assessing vine vigor growth status show a negative correlation with grape TSS from veraison to harvest stage. This is because vine vigor has an negative impact on grape quality [33]. However, most of VIs show a weak correlation with grape TSS during veraison stage. In addition, the simple linear relationship between each of the 23 VIs and grape TSS were explored. The result showed that OSAVI had the best linear correlation with grape TSS with a R^2 of 0.4 and RMSE of 0.89 °Brix (Appendix A). This was followed by RDVI, ARI, EVI, MSAVI, and NGBDI (Appendix A). The OSAVI is calculated based on NIR and red bands; this suggests that OSAVI is a promising candidate to predict the grape TSS when multispectral sensors are available. The promising performance of NGBDI implies that, when only RGB sensors are available, NGBDI may serve as a spectral indicator for grape TSS.

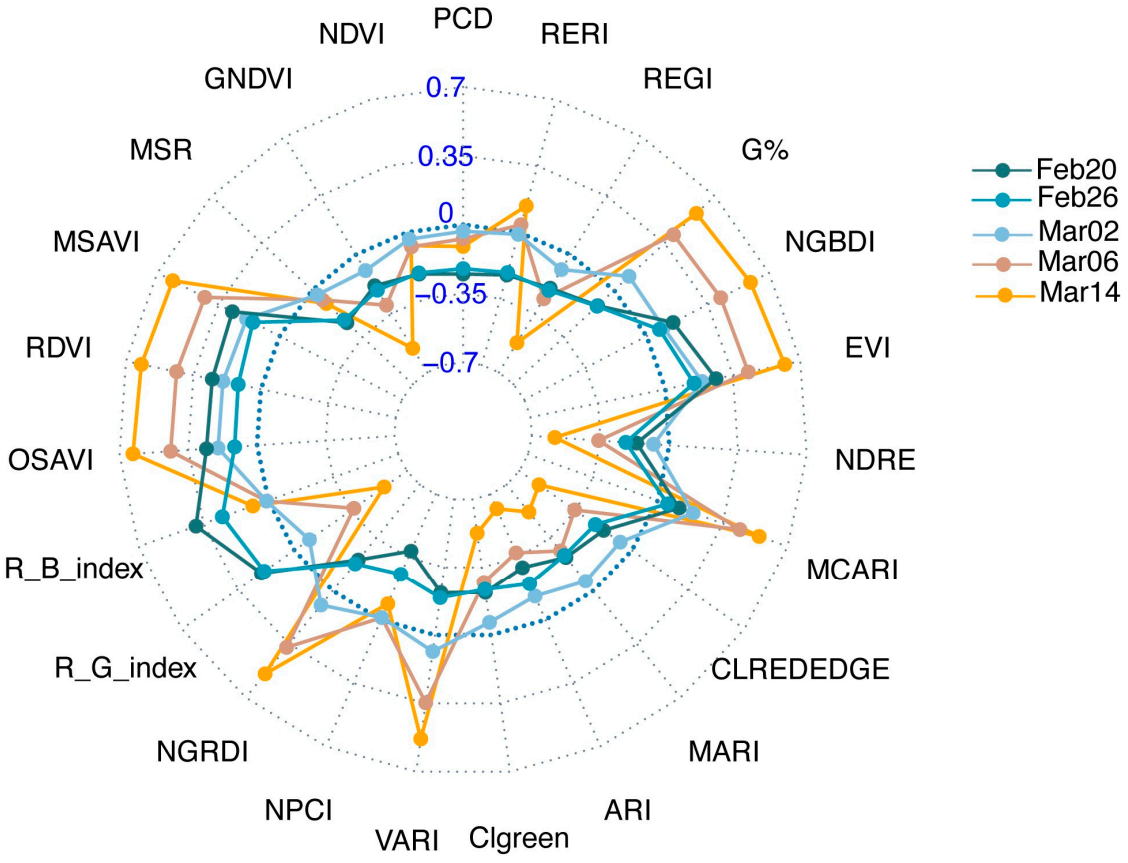

Figure 5. Pearson's correlation coefficient between VIs and grape TSS (Different colors represent different sampling date).

3.3. Spatial Variability of Soil EC_a, Elevation and Vine Vigour Status

The geostatistical analysis was used to map the spatial variation in soil EC_a, elevation, and vine vigor status within the vineyard. Soil EC_a was measured at 0.5 m depth by an EM38-MK2. The kriging interpolation maps showed the spatial variability of soil EC_a, elevation, and vine vigour status within the vineyard (Figures 6 and 7). In the PN vineyard, soil EC_a values showed lower values in the northeastern portion, higher values in a small portion of the eastern region, and the south-western border (Figure 6a). In the HN vineyard, soil EC_a values were low in the south-western section of the vineyard, and in the north-eastern section showed high soil EC_a values (Figure 7a). When it turns to elevation, elevation values were high in the south-eastern region and low in the north-western region in PN (Figure 6b). In the HN vineyard, elevation values were higher in the middle region and lower in the north-eastern region. The trunk circumference, NDVI and PCD were used to represent the vine vigour status in many studies [21]. Figures 6c and 7c show the spatial variation in TC within study sites. In the PN vineyard, TC values were lower in the south-eastern boundary region and higher in the north-western region (Figure 6c). In HN vineyard, TC values were low in the north-eastern boundary region and high in the northern region (Figure 7c). When it turns to NDVI and PCD, the spatial pattern of these two VIs is similar in each vineyard (Figures 6 and 7). In PN, NDVI and PCD showed high value in the south-western and north-eastern corner, while the low value show in middle region (Figure 6d,e). In HN, NDVI and PCD showed high value in the south-eastern boundary, and low value in the northern region. (Figure 7d,e)

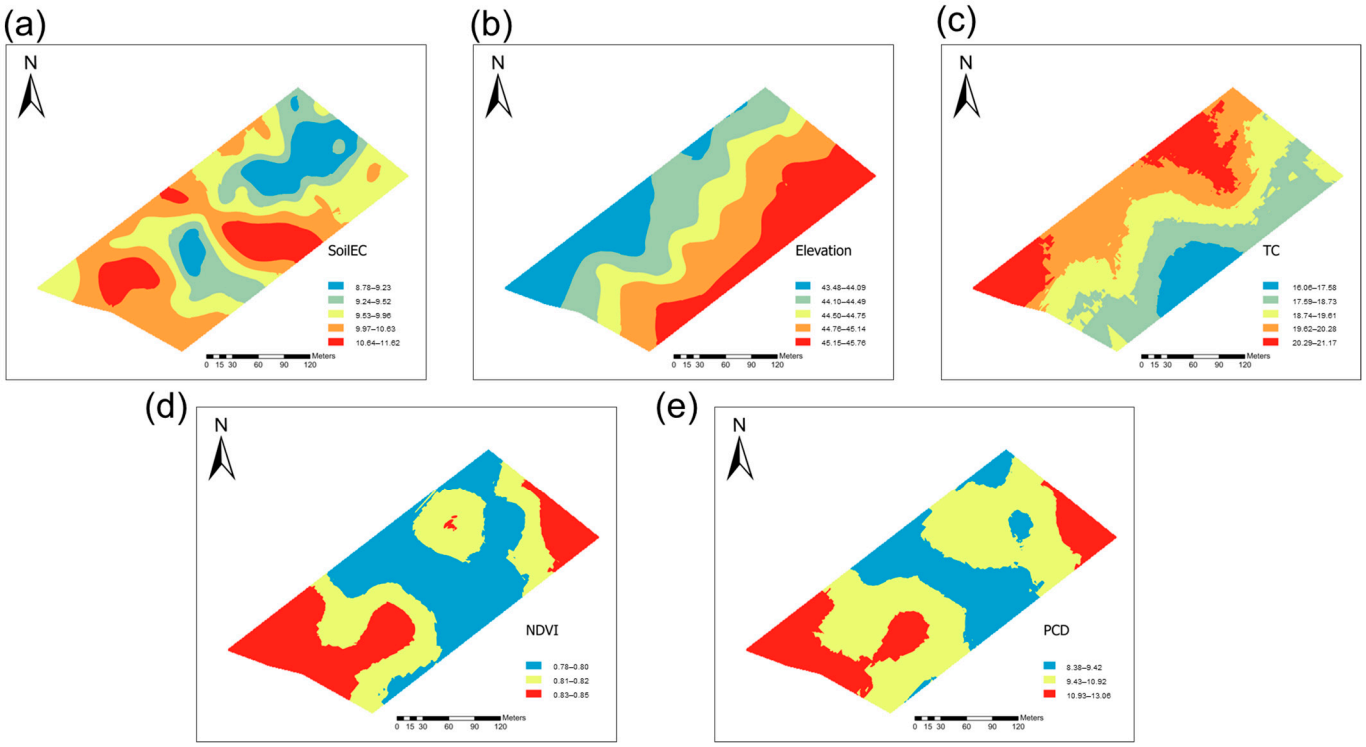

Figure 6. Spatial interpolation map of soil EC_a (**a**); elevation (**b**); trunk circumference (**c**); NDVI (**d**); PCD (**e**) in PN vineyard.

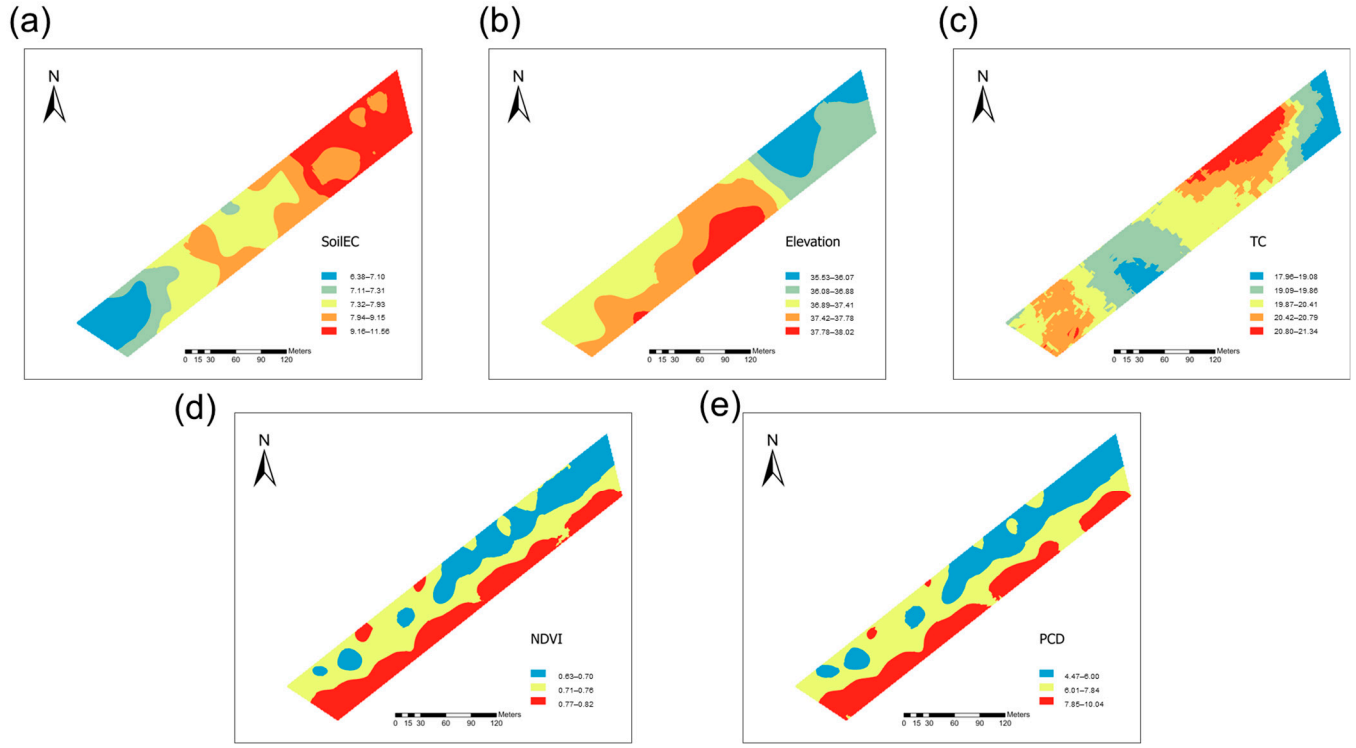

Figure 7. Spatial interpolation map of soil EC_a (**a**); elevation (**b**); trunk circumference (**c**); NDVI (**d**); PCD (**e**) in HN vineyard.

3.4. Prediction Model Performance of Grape TSS

The machine learning models used both linear and nonlinear regression analysis to predict grape TSS. The input variable includes all 23 VIs obtained from UAV imagery, NDVI_proximal, and soil EC_a obtained from proximal sensor, elevation, and slope obtained from a LiDAR camera, as well as TC obtained directly in the vineyards. In order to ensure the robustness and generalization of the models used in this study, the model evaluation process was repeated 20 times with different data splits. When using linear regression models, the best prediction model is ridge regression with an average R^2 of 0.31 and RMSE of 1.43 °Brix, respectively (Table 4). For lasso regression, the average result of predicting TSS were a R^2 of 0.3 and a RMSE of 1.44 °Brix, respectively (Table 4).

Table 4. The prediction performance of study machine learning models (bold represents the best prediction performance).

Method	R^2	RMSE
Lasso regression	0.3 ± 0.08	1.44 ± 0.1
Ridge regression	0.31 ± 0.08	1.43 ± 0.1
KNN	0.24 ± 0.08	1.5 ± 0.1
SVR	0.37 ± 0.08	1.38 ± 0.09
RFR	**0.52 ± 0.06**	**1.19 ± 0.07**
XGBoost	0.52 ± 0.06	1.2 ± 0.09
ANN	0.31 ± 0.11	1.43 ± 0.13

Among the nonlinear methods, this study evaluated the prediction performance of the individual machine learning models (KNN, SVR), ensemble learning methods (RFR, XGBoost), and deep learning method (ANN) to estimate grape TSS. The ensemble machine learning methods including RFR and XGBoost improved the prediction performance (Table 4). The best prediction performance for the nonlinear methods was the RFR algorithm with an average R^2 of 0.52 and RMSE of 1.19 °Brix, respectively (Table 4). The

result of using XGBoost showed a similar prediction performance with RFR (R^2 = 0.52, RMSE = 1.2 °Brix). RFR and XGBoost aggregated the predictions from multiple decision trees together, to significantly improve the estimation accuracy than the other machine learning models (Figure 8). However, the KNN model showed a significantly poor prediction accuracy compared with other linear and nonlinear regression models with an average R^2 of 0.24 and RMSE of 1.2 °Brix (Table 4 and Figure 8). Compared with the linear regression models, SVR significantly improved the prediction performance with an average R^2 of 0.37 and RMSE of 1.38 °Brix (Table 4 and Figure 8). However, ANN showed a similar prediction performance as linear regression model with an average R^2 of 0.31 and RMSE of 1.43 °Brix (Table 4 and Figure 8).

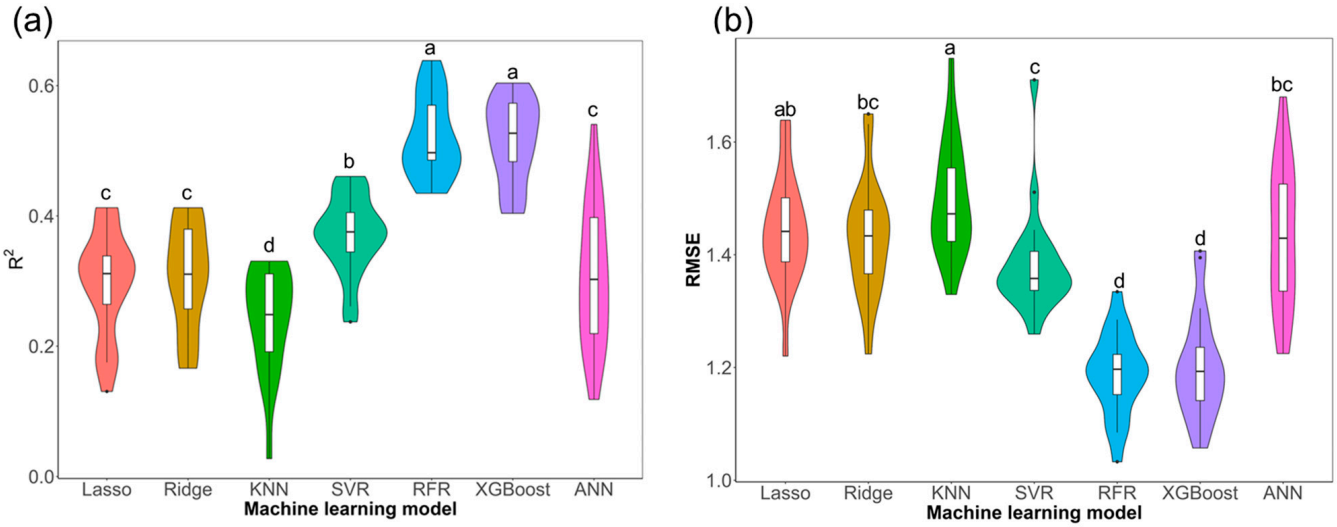

Figure 8. The boxplot of different machine learning model performance in R^2 (**a**); RMSE (**b**). (Different letters between any two groups represents significant difference between them, if two groups have the same letter then this indicates that they are not statistically different).

In order to reduce redundant information from the 23 VIs, OSAVI and NGBDI were used as the main input for different machine learning models with other ancillary variables. OSAVI and NGBDI consider the different scenarios of available sensors, in order to better target practical applications. Compared to regression using all 23 VIs, the result of most of the machine learning models increased when using OSAVI-based model or NGBDI-based model (Tables 4–6). When using OSAVI-based models, the best prediction model is RFR with an average R^2 of 0.51 and RMSE of 1.19 °Brix, respectively (Table 5). For NGBDI-based model, the RFR model showed the best average result predicting TSS with an R^2 of 0.54 and a RMSE of 1.16 °Brix, respectively (Table 6). Figures 9 and 10 showed that the variation of different machine learning models' performance during the repeated 20 times different data splits strategies. The result of Waller–Duncan showed that using ensemble learning models (RFR and XGBoost) demonstrated greater capability than that of lasso, ridge, KNN, and SVR (Figures 9 and 10). Figure A1 plots the regression relationship between the best predicted values and actual values for the best performance model (NGBDI-based RFR model).

Table 5. The predicted performance of OSAVI-based models (bold represents the best prediction performance).

Method	R^2	RMSE
Lasso regression	0.3 ± 0.08	1.44 ± 0.1
Ridge regression	0.32 ± 0.1	1.38 ± 0.1
KNN	0.4 ± 0.07	1.3 ± 0.1
SVR	0.36 ± 0.07	1.39 ± 0.1
RFR	**0.51 ± 0.07**	**1.19 ± 0.07**
XGBoost	0.5 ± 0.07	1.21 ± 0.08
ANN	0.45 ± 0.12	1.26 ± 0.14

Table 6. The predicted performance of NGBDI-based models (bold represents the best prediction performance).

Method	R^2	RMSE
Lasso regression	0.3 ± 0.08	1.43 ± 0.09
Ridge regression	0.32 ± 0.1	1.43 ± 0.09
KNN	0.4 ± 0.06	1.31 ± 0.1
SVR	0.4 ± 0.07	1.33 ± 0.12
RFR	**0.54 ± 0.07**	**1.16 ± 0.07**
XGBoost	0.52 ± 0.06	1.19 ± 0.07
ANN	0.39 ± 0.11	1.31 ± 0.11

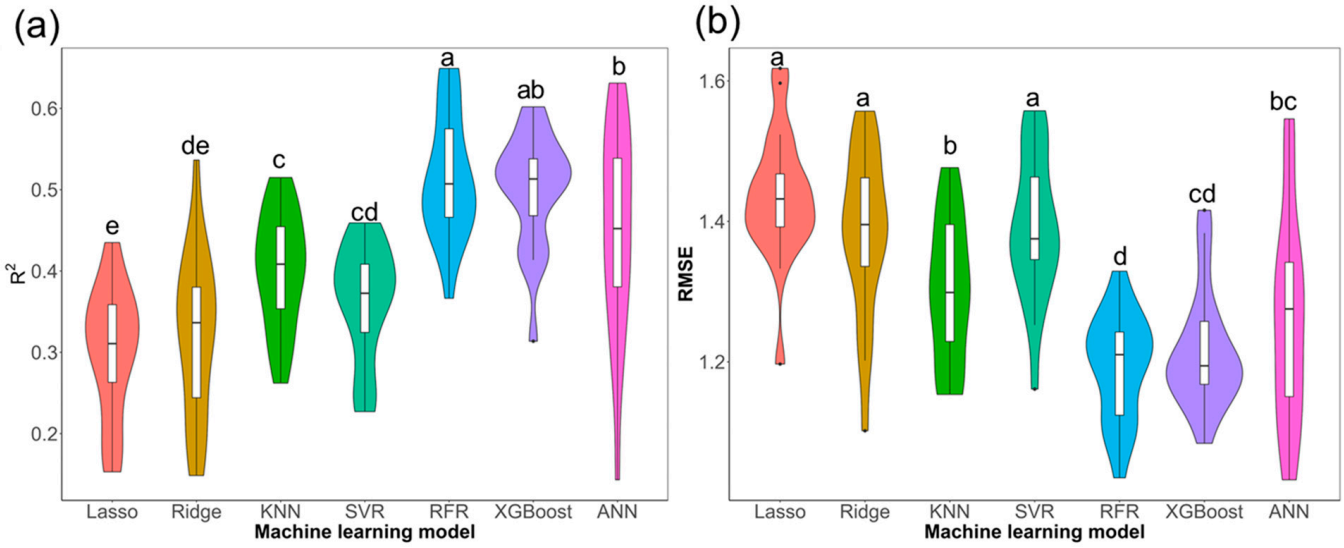

Figure 9. The boxplot of different OSAVI-based model performance in R^2 (**a**); RMSE (**b**). (Different letters between any two groups represents significant difference between them, if two groups have the same letter then this indicates that they are not statistically different).

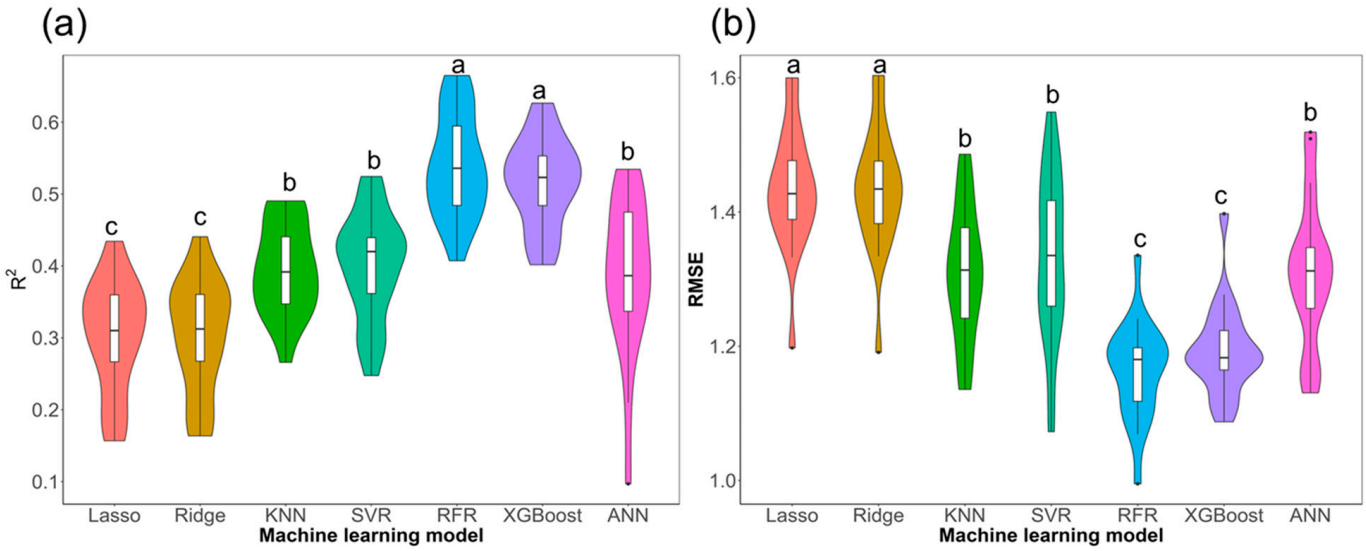

Figure 10. The boxplot of different NGBDI-based model performance in R^2 (**a**); RMSE (**b**). (Different letters between any two groups represents significant difference between them, if two groups have the same letter then this indicates that they are not statistically different).

4. Discussion

In this study, we explored the potential to use VIs, soil EC_a, elevation, slope, and TC data as input variables to predict the grape sugar content in a non-destructive way. A total of 236 samples from Pinot Noir cultivars had the TSS measured values based on destructive methods from two commercial vineyards and used as output variable in the regression model. The grape TSS was measured on five different days in the period from veraison to harvest. During the veraison stage, the berries start to mature changing color, softening, accumulating sugar, and reducing acid [37]. From veraison, grape growers start to measure the grape quality parameters such as TSS, pH, and titratable acidity in order to determine the best harvest day. Among them, the TSS is an important parameter to assess the grape maturity as it can determine the alcohol concentration and flavor of the subsequent wine. Figure 4 shows that the sugar content of grapes initially decreased and then increased during the study period. However, in a previous study, the sugar concentration of grapes exhibited a strong increase starting from veraison and eventually reached a plateau during harvest stage [38]. One possible reason is that the sampling vines were randomly selected during each of the five-measurement days, without repeating the selection. This differed from the sampling strategy used in the previous study. Several studies have shown that there is considerable spatial and temporal variation in grape TSS [2,39]. Thus, the grapes in different geographic locations may accumulate sugar at different rates [2]. On each measurement day, the large magnitude of the interquartile range and the outlier in Figure 4 showed the large spatial variability in grape TSS within the vineyard blocks. Thus, it is inappropriate to take a single or average measurements, collected in the vineyard to represent the grape maturity stage.

Due to the spatial variability of grape quality at the vineyard scale, it is important to measure the grape quality across the entire vineyard. However, the traditional method relies on destructive measurement, which makes it impossible to measure each grape berry's quality. Thus many studies have explored the potential of using advanced sensing techniques to measure the grape quality with a non-destructive method [15,17,18,40]. However, most of these studies used direct measurements of berries or clusters to estimate grape quality parameters [15,17,31]. Few studies have predicted grape quality by canopy or at the leaf level [18]. In this study we propose an alternative method to predict grape TSS based on VIs and other ancillary data. Different biological stress conditions can cause changes in canopy status such as heightened pigment levels or canopy structure change,

which will affect the quality of subsequent berries. These changes can affect the way plants interact with light of different wavelengths [41]. Based on these characteristics, many studies have used hyperspectral and multispectral images to predict the crop growth status, yield and quality [14]. Compared with hyperspectral cameras, this study used a cheaper multispectral UAV imaging system to acquire the canopy reflectance data in the red, red edge, blue, green, and near-infrared bands. The red, red edge, and near infrared bands have been reported to be related with the chlorophyll content and leaf structure. The blue and green bands have been proven to be associated with the canopy pigments change. In this study, we calculated 23 VIs based on different bands reflectance data values. Due to the grape TSS being measured from different locations without a repeat at each sampling date, the data was grouped based on measurement date, and the Pearson's coefficient calculated between VIs and grape TSS in each group (Figure 5). A previous study calculated the Pearson's correlation coefficient between spectral indices acquired from UAV RGB imagery and grape quality parameters [12]. The result found significant correlations between berry weight, malic acid, alpha amino nitrogen, phenolic maturation index, total polyphenol index, and spectral indices. However, the spectral indices calculated from RGB imagery show a poor correlation with TSS in their study. In this study, multispectral cameras can provide additional spectral values in the near infrared and red-edge band. The VIs including OSAVI, RDVI, EVI, ARI, and MSAVI which are computed based on the spectral bands including near infrared and red edge, which showed a strong correlation between grape TSS during the harvest stage (Figure 5). Furthermore, the simple linear regression between each of the 23 VIs and grape TSS during harvest stage was examined. It is apparent that the prediction performance of using only RGB bands was lower than that of using the VIs which combined with near infrared and red edge bands.

The MSAVI, RDVI, and OSAVI were calculated from different wavelength reflectance in the red and near infrared bands. Red and near infrared band are the most common band combination to monitor biomass and vegetation density as well as biophysical parameters [42]. PCD and NDVI calculated based on the reflectance value in red and near infrared band were widely used in PV [18,21,43,44]. For example, one study used PCD as an indicator to represent the vine vigor and explore their spatial variability within vineyard [43]. In addition, the NDVI are commonly used to identify the vine row space using high spatial resolution imagery [45]. Due to the discontinuity of the vegetation surface in the vineyard, it is necessary to extract the vegetation information from the vine canopy under the high-resolution images, to reduce the influence of soil and weeds between rows. In this study, a simple threshold method on NDVI and DSM-DTM was used to identify the vine row area. However, the Pearson's correlation coefficient between NDVI and grape TSS is low in this study. A previous study showed that the NDVI obtained at veraison stage to have a strong correlation with grape TSS [18]. One possible reason is that the UAV imagery was acquired during the flowering stage. Most studies showed that there was a strong correlation between NDVI and grape quality parameters at the late development stages of vine growing [46,47]. It is worth noting that the vineyard will use the antibird net to protect the grapes after veraison. This makes it difficult to use UAV and satellites to obtain accurate canopy reflection data during this period.

Furthermore, the potential of using machine learning models to predict the grape TSS was evaluated. In addition to the VIs collected during flowering, the input variables in the machine learning includes the NDVI_proximal value measured on a handheld proximal sensor during the post veraison stage, the soil EC_a value measured from EM38-MK2, elevation and slope value obtained from LiDAR data, and TC measured in the field. The dataset was used to train and test machine learning models, evaluating the performance of linear and nonlinear regression models including lasso regression, ridge regression, KNN, SVR, RFR, XGBoost, and ANN. When we used all input variables in machine learning models, the ensemble method, which included RFR and XGBoost showed similar prediction accuracy for grape TSS prediction, with the best-fitted model achieving R^2 = 0.52 and RMSE = 1.19 °Brix. These results confirm the findings of [18], who compared the linear and

nonlinear regression models in predicting grape TSS, and they concluded that the AdaBoosting, RFR, and Extra Trees model outperform the other machine learning models [18]. In addition, another study showed that the XGBoost and RFR demonstrated greater capability for modeling crop yield than linear regression model and ANN [48]. Compared with [48], this study tested different machine learning models, 20 times with different test sets, and used Waller–Duncan to analyze the differences between the performance of each model. Furthermore, this study used OSAVI or NGBDI as main input variables with other ancillary data to predict grape TSS based on different machine learning models. We chose OSAVI and NGBDI as the main input variables, as they represent the Vis that can be obtained when different sensors are available. Similar results were obtained with 23 VIs used as input variables, the RFR showed the best prediction performance (Tables 4–6). Therefore, the implementation of ensemble learning techniques provide potential to predict the grape TSS in a non-destructive way, based on remote sensed data. However, it should be noted that berry quality was affected by the environmental conditions during the harvest stage (e.g., radiation, temperature). A further study should continue to explore relationships, using different input variables to predict grape TSS. In addition, the berry samples were only 3 berries per vine which cannot represent the whole vine grapes' TSS value but was used to return a range of TSS values. The sample size may influence the prediction performance when using different machine learning models. Thus, further study should increase the berry sampling numbers.

5. Conclusions

This study investigates the possibility of using the combination of remote and proximal sensed data and machine learning techniques to predict the wine grape quality parameter used as a proxy for TSS. The Pearson's correlation coefficient showed that the VIs obtained from the UAV during the flowering stage have a strong correlation with the grape TSS during the harvest stage. The input variables, which include VIs obtained from UAV, NDVI, and soil EC_a obtained from proximal sensors, elevation, and slope obtained from a LiDAR camera, as well as TC obtained directly in the vineyard, was used to build regression models to estimate grape TSS in a non-destructive way. This study evaluates the prediction performance of seven machine learning techniques: ridge regression, lasso regression, KNN, SVR, RFR, XGBoost, and ANN. The result shows that ensemble learning models (RFR and XGBoost) outperform other regression models when predicting grape TSS. This study develops an alternative approach to predict the grape TSS by different predictor values through various advanced techniques. For grape growers, the approach developed in this study could help them assess the whole vineyard grape TSS in a non-destructive way, in order to make the harvest decision.

Author Contributions: Conceptualization, H.L. and M.G.; methodology, H.L., T.R., M.G. and M.I.; software, H.L., M.I. and E.S.; validation, H.L., T.R., M.I. and E.S.; formal analysis, H.L.; investigation, H.L., E.S., T.R. and M.I.; resources, M.G. and E.S.; data curation, H.L., H.-E.W., M.I. and E.S.; writing—original draft preparation, H.L.; writing—review and editing, M.G. and T.R.; visualization, H.L. and M.I.; supervision, M.G., T.R. and M.I.; project administration, M.G.; funding acquisition, M.G. All authors have read and agreed to the published version of the manuscript.

Funding: This research received no external funding.

Data Availability Statement: The data presented in this study are available on request from the corresponding author.

Acknowledgments: We acknowledge the assistance of Guy McMaster, Manager, and Wine Maker of Palliser Winery.

Conflicts of Interest: The authors declare no conflict of interest.

Appendix A

Table A1. R^2 and RMSE based on a linear regression between TSS and each Vis during 14 March.

Vis	R^2	RMSE	Date
OSAVI	0.40	0.89	14 March
RDVI	0.38	0.90	14 March
ARI	0.38	0.90	14 March
EVI	0.38	0.90	14 March
MSAVI	0.38	0.90	14 March
NGBDI	0.35	0.92	14 March
NDRE	0.34	0.93	14 March
CLREDEDGE	0.33	0.93	14 March
G%	0.33	0.94	14 March
R_G_index	0.31	0.95	14 March
GNDVI	0.31	0.95	14 March
MCARI	0.30	0.96	14 March
NGRDI	0.30	0.96	14 March
VARI	0.28	0.97	14 March
Clgreen	0.28	0.97	14 March
REGI	0.27	0.97	14 March
MARI	0.27	0.98	14 March
RERI	0.02	1.13	14 March
PCD	0.01	1.14	14 March
MSR	0.01	1.14	14 March
R_B_index	0.01	1.14	14 March
NDVI	0.01	1.14	14 March
OSAVI	0.40	0.89	14 March

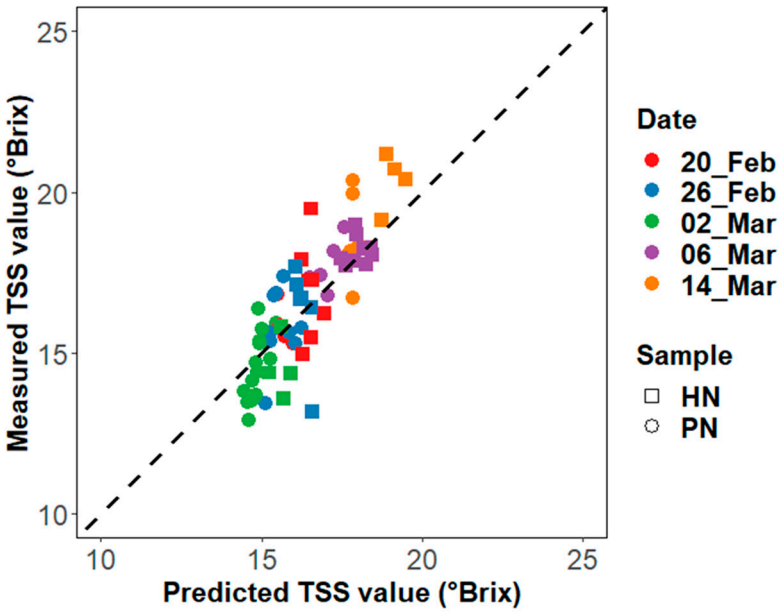

Figure A1. Measured TSS value comparison against predicted TSS value for the best NGBDI-based RFR model.

References

1. *Vineyard Report 2022 New Zealand Winegrowers*; New Zealand Winegrowers: Auckland, New Zealand, 2022; pp. 1–22.
2. Baluja, J.; Tardaguila, J.; Ayestaran, B.; Diago, M.P. Spatial Variability of Grape Composition in a Tempranillo (*Vitis vinifera* L.) Vineyard over a 3-Year Survey. *Precis. Agric.* **2013**, *14*, 40–58. [CrossRef]
3. Bramley, R.G.V.; Trought, M.C.; Praat, J.-P. Vineyard Variability in Marlborough, New Zealand: Characterising Variation in Vineyard Performance and Options for the Implementation of Precision Viticulture. *Aust. J. Grape Wine Res.* **2011**, *17*, 72–78. [CrossRef]

4. Froment, M.; Dampney, P.; Goodlass, G.; Dawson, C.; Clarke, J. *A Review of Spatial Variation of Nutrients in Soil*; MAFF final report for project CE0139; Ministry of Agriculture, Fisheries and Food: London, UK, 1995.
5. Wei, H.-E.; Grafton, M.; Bretherton, M.; Irwin, M.; Sandoval, E. Evaluation of the Use of Two-Stage Calibrated PlanetScope Images and Environmental Variables for the Development of the Grapevine Water Status Prediction Model. *Technol. Agron.* **2023**, *3*, 6. [CrossRef]
6. Rey-Caramés, C.; Diago, M.P.; Martín, M.P.; Lobo, A.; Tardaguila, J. Using RPAS Multi-Spectral Imagery to Characterise Vigour, Leaf Development, Yield Components and Berry Composition Variability within a Vineyard. *Remote Sens.* **2015**, *7*, 14458–14481. [CrossRef]
7. Lamb, D.W.; Weedon, M.M.; Bramley, R.G.V. Using Remote Sensing to Predict Grape Phenolics and Colour at Harvest in a Cabernet Sauvignon Vineyard: Timing Observations against Vine Phenology and Optimising Image Resolution. *Aust. J. Grape Wine Res.* **2004**, *10*, 46–54. [CrossRef]
8. Arab, S.T.; Ahamed, T. Land Suitability Analysis for Potential Vineyards Extension in Afghanistan at Regional Scale Using Remote Sensing Datasets. *Remote Sens.* **2022**, *14*, 4450. [CrossRef]
9. Arab, S.T.; Noguchi, R.; Matsushita, S.; Ahamed, T. Prediction of Grape Yields from Time-Series Vegetation Indices Using Satellite Remote Sensing and a Machine-Learning Approach. *Remote Sens. Appl. Soc. Environ.* **2021**, *22*, 100485. [CrossRef]
10. Carrillo, E.; Matese, A.; Rousseau, J.; Tisseyre, B. Use of Multi-Spectral Airborne Imagery to Improve Yield Sampling in Viticulture. *Precis. Agric.* **2016**, *17*, 74–92. [CrossRef]
11. Matese, A.; Toscano, P.; Di Gennaro, S.F.; Genesio, L.; Vaccari, F.P.; Primicerio, J.; Belli, C.; Zaldei, A.; Bianconi, R.; Gioli, B. Intercomparison of UAV, Aircraft and Satellite Remote Sensing Platforms for Precision Viticulture. *Remote Sens.* **2015**, *7*, 2971–2990. [CrossRef]
12. García-Fernández, M.; Sanz-Ablanedo, E.; Rodríguez-Pérez, J.R. High-Resolution Drone-Acquired RGB Imagery to Estimate Spatial Grape Quality Variability. *Agronomy* **2021**, *11*, 655. [CrossRef]
13. Wei, H.-E.; Grafton, M.; Bretherton, M.; Irwin, M.; Sandoval, E. Evaluation of the Use of UAV-Derived Vegetation Indices and Environmental Variables for Grapevine Water Status Monitoring Based on Machine Learning Algorithms and SHAP Analysis. *Remote Sens.* **2022**, *14*, 5918. [CrossRef]
14. Lyu, H.; Grafton, M.; Ramilan, T.; Irwin, M.; Sandoval, E. Assessing the Leaf Blade Nutrient Status of Pinot Noir Using Hyperspectral Reflectance and Machine Learning Models. *Remote Sens.* **2023**, *15*, 1497. [CrossRef]
15. Kalopesa, E.; Karyotis, K.; Tziolas, N.; Tsakiridis, N.; Samarinas, N.; Zalidis, G. Estimation of Sugar Content in Wine Grapes via In Situ VNIR–SWIR Point Spectroscopy Using Explainable Artificial Intelligence Techniques. *Sensors* **2023**, *23*, 1065. [CrossRef] [PubMed]
16. Bramley, R.; Pearse, B.; Chamberlain, P. Being Profitable Precisely-A Case Study of Precision Viticulture from Margaret River. *Aust. New Zealand Grapegrow. Winemak. [Annu. Tech. Issue]* **2003**, *473a*, 84–87.
17. Benelli, A.; Cevoli, C.; Ragni, L.; Fabbri, A. In-Field and Non-Destructive Monitoring of Grapes Maturity by Hyperspectral Imaging. *Biosyst. Eng.* **2021**, *207*, 59–67. [CrossRef]
18. Kasimati, A.; Espejo-Garcia, B.; Vali, E.; Malounas, I.; Fountas, S. Investigating a Selection of Methods for the Prediction of Total Soluble Solids among Wine Grape Quality Characteristics Using Normalized Difference Vegetation Index Data from Proximal and Remote Sensing. *Front. Plant Sci.* **2021**, *12*, 683078. [CrossRef] [PubMed]
19. Dambergs, R.; Gishen, M.; Cozzolino, D. A Review of the State of the Art, Limitations, and Perspectives of Infrared Spectroscopy for the Analysis of Wine Grapes, Must, and Grapevine Tissue. *Appl. Spectrosc. Rev.* **2015**, *50*, 261–278. [CrossRef]
20. Kasimati, A.; Espejo-García, B.; Darra, N.; Fountas, S. Predicting Grape Sugar Content under Quality Attributes Using Normalized Difference Vegetation Index Data and Automated Machine Learning. *Sensors* **2022**, *22*, 3249. [CrossRef]
21. Bramley, R.G.V. Precision Viticulture: Managing Vineyard Variability for Improved Quality Outcomes. In *Managing Wine Quality*; Elsevier: Amsterdam, The Netherlands, 2022; pp. 541–586.
22. Arnó Satorra, J.; Martínez Casasnovas, J.A.; Ribes Dasi, M.; Rosell Polo, J.R. Precision Viticulture. Research Topics, Challenges and Opportunities in Site-Specific Vineyard Management. *Span. J. Agric. Res.* **2009**, *7*, 779–790. [CrossRef]
23. Rouse, J.W., Jr.; Haas, R.H.; Deering, D.W.; Schell, J.A.; Harlan, J.C. *Monitoring the Vernal Advancement and Retrogradation (Green Wave Effect) of Natural Vegetation*; National Aeronautics and Space Administration: Washington, DC, USA, 1974; pp. 1–120.
24. Romero, M.; Luo, Y.; Su, B.; Fuentes, S. Vineyard Water Status Estimation Using Multispectral Imagery from an UAV Platform and Machine Learning Algorithms for Irrigation Scheduling Management. *Comput. Electron. Agric.* **2018**, *147*, 109–117. [CrossRef]
25. Gil-Pérez, B.; Zarco-Tejada, P.J.; Correa-Guimaraes, A.; Relea-Gangas, E.; Navas-Gracia, L.M.; Hernández-Navarro, S.; Sanz-Requena, J.F.; Berjón, A.; Martín-Gil, J. Remote Sensing Detection of Nutrient Uptake in Vineyards Using Narrow-Band Hyperspectral Imagery. *Vitis* **2010**, *49*, 167–173.
26. Jiménez-Brenes, F.M.; Lopez-Granados, F.; Torres-Sánchez, J.; Peña, J.M.; Ramírez, P.; Castillejo-González, I.L.; de Castro, A.I. Automatic UAV-Based Detection of Cynodon Dactylon for Site-Specific Vineyard Management. *PLoS ONE* **2019**, *14*, e0218132. [CrossRef] [PubMed]
27. Brook, A.; De Micco, V.; Battipaglia, G.; Erbaggio, A.; Ludeno, G.; Catapano, I.; Bonfante, A. A Smart Multiple Spatial and Temporal Resolution System to Support Precision Agriculture from Satellite Images: Proof of Concept on Aglianico Vineyard. *Remote Sens. Environ.* **2020**, *240*, 111679. [CrossRef]

28. Albetis, J.; Duthoit, S.; Guttler, F.; Jacquin, A.; Goulard, M.; Poilvé, H.; Féret, J.-B.; Dedieu, G. Detection of Flavescence Dorée Grapevine Disease Using Unmanned Aerial Vehicle (UAV) Multispectral Imagery. *Remote Sens.* **2017**, *9*, 308. [CrossRef]
29. Soubry, I.; Patias, P.; Tsioukas, V. Monitoring Vineyards with UAV and Multi-Sensors for the Assessment of Water Stress and Grape Maturity. *J. Unmanned Veh. Syst.* **2017**, *5*, 37–50. [CrossRef]
30. Cogato, A.; Pagay, V.; Marinello, F.; Meggio, F.; Grace, P.; De Antoni Migliorati, M. Assessing the Feasibility of Using Sentinel-2 Imagery to Quantify the Impact of Heatwaves on Irrigated Vineyards. *Remote Sens.* **2019**, *11*, 2869. [CrossRef]
31. Pádua, L.; Marques, P.; Hruška, J.; Adão, T.; Bessa, J.; Sousa, A.; Peres, E.; Morais, R.; Sousa, J.J. Vineyard Properties Extraction Combining UAS-Based RGB Imagery with Elevation Data. *Int. J. Remote Sens.* **2018**, *39*, 5377–5401. [CrossRef]
32. Albetis, J.; Jacquin, A.; Goulard, M.; Poilvé, H.; Rousseau, J.; Clenet, H.; Dedieu, G.; Duthoit, S. On the Potentiality of UAV Multispectral Imagery to Detect Flavescence Dorée and Grapevine Trunk Diseases. *Remote Sens.* **2018**, *11*, 23. [CrossRef]
33. Bramley, R.G.V.; Ouzman, J.; Boss, P.K. Variation in Vine Vigour, Grape Yield and Vineyard Soils and Topography as Indicators of Variation in the Chemical Composition of Grapes, Wine and Wine Sensory Attributes. *Aust. J. Grape Wine Res.* **2011**, *17*, 217–229. [CrossRef]
34. SU, S.L.; Singh, D.N.; Baghini, M.S. A Critical Review of Soil Moisture Measurement. *Measurement* **2014**, *54*, 92–105. [CrossRef]
35. Trought, M.C.; Dixon, R.; Mills, T.; Greven, M.; Agnew, R.; Mauk, J.L.; Praat, J.-P. The Impact of Differences in Soil Texture within a Vineyard on Vine Vigour, Vine Earliness and Juice Composition. *OENO One* **2008**, *42*, 67–72. [CrossRef]
36. Yu, R.; Brillante, L.; Martínez-Lüscher, J.; Kurtural, S.K. Spatial Variability of Soil and Plant Water Status and Their Cascading Effects on Grapevine Physiology Are Linked to Berry and Wine Chemistry. *Front. Plant Sci.* **2020**, *11*, 790. [CrossRef] [PubMed]
37. Keller, M. *The Science of Grapevines*; Academic Press: Cambridge, MA, USA, 2020; ISBN 0-12-816702-5.
38. Trought, M.C.; Bramley, R.G. Vineyard Variability in Marlborough, New Zealand: Characterising Spatial and Temporal Changes in Fruit Composition and Juice Quality in the Vineyard. *Aust. J. Grape Wine Res.* **2011**, *17*, 79–89. [CrossRef]
39. Bramley, R.G.V. Understanding Variability in Winegrape Production Systems 2. Within Vineyard Variation in Quality over Several Vintages. *Aust. J. Grape Wine Res.* **2005**, *11*, 33–42. [CrossRef]
40. Gomes, V.M.; Fernandes, A.M.; Faia, A.; Melo-Pinto, P. Comparison of Different Approaches for the Prediction of Sugar Content in New Vintages of Whole Port Wine Grape Berries Using Hyperspectral Imaging. *Comput. Electron. Agric.* **2017**, *140*, 244–254. [CrossRef]
41. Sanches, I.D.; Souza Filho, C.R.; Kokaly, R.F. Spectroscopic Remote Sensing of Plant Stress at Leaf and Canopy Levels Using the Chlorophyll 680 Nm Absorption Feature with Continuum Removal. *ISPRS J. Photogramm. Remote Sens.* **2014**, *97*, 111–122. [CrossRef]
42. Giovos, R.; Tassopoulos, D.; Kalivas, D.; Lougkos, N.; Priovolou, A. Remote Sensing Vegetation Indices in Viticulture: A Critical Review. *Agriculture* **2021**, *11*, 457. [CrossRef]
43. Bramley, R.G.V.; Ouzman, J.; Trought, M.C.; Neal, S.M.; Bennett, J.S. Spatio-temporal Variability in Vine Vigour and Yield in a Marlborough Sauvignon Blanc Vineyard. *Aust. J. Grape Wine Res.* **2019**, *25*, 430–438. [CrossRef]
44. Proffitt, T.; Malcolm, A. Implementing Zonal Vineyard Management through Airborne Remote Sensing. *Aust. New Zealand Grapegrow. Winemak.* **2005**, 22–31.
45. Hall, A.; Louis, J.; Lamb, D. Characterising and Mapping Vineyard Canopy Using High-Spatial-Resolution Aerial Multispectral Images. *Comput. Geosci.* **2003**, *29*, 813–822. [CrossRef]
46. Anastasiou, E.; Balafoutis, A.; Darra, N.; Psiroukis, V.; Biniari, A.; Xanthopoulos, G.; Fountas, S. Satellite and Proximal Sensing to Estimate the Yield and Quality of Table Grapes. *Agriculture* **2018**, *8*, 94. [CrossRef]
47. Sun, L.; Gao, F.; Anderson, M.C.; Kustas, W.P.; Alsina, M.M.; Sanchez, L.; Sams, B.; McKee, L.; Dulaney, W.; White, W.A. Daily Mapping of 30 m LAI and NDVI for Grape Yield Prediction in California Vineyards. *Remote Sens.* **2017**, *9*, 317. [CrossRef]
48. Jiang, G.; Grafton, M.C.; Pearson, D.; Bretherton, M.R.; Holmes, A. A Comparison of Supervised Machine Learning Algorithms for Predicting Subfield Yield Variability of Maize Grain. *J. ASABE* **2022**, *65*, 287–294. [CrossRef]